Int. J. Radiation Oncology Biol. Phys., Vol. 63, No. 3, pp. 901–910, 2005

0360-3016/05/$–see front matter

ELSEVIER

doi:10.1016/j.ijrobp.2005.02.038

BIOLOGY CONTRIBUTION

EARLY REOXYGENATION IN TUMORS AFTER IRRADIATION: DETERMINING FACTORS AND CONSEQUENCES FOR RADIOTHERAPY REGIMENS USING DAILY MULTIPLE FRACTIONS

Nathalie Crokart, M.Sc.,*† Bénédicte F. Jordan, Ph.D.,*† Christine Baudelet, Ph.D.,*† Reginald Ansiaux, M.Sc.,*† Pierre Sonveaux, Ph.D.,‡ Vincent Grégoire, M.D., Ph.D.,§ Nelson Beghein, B.Sc.,*† Julie DeWever, B.Sc.,§ Caroline Bouzin, Ph.D.,§ Olivier Feron, Ph.D.,§ and Bernard Gallez, Ph.D.*†

*Laboratory of Medicinal Chemistry and Radiopharmacy, †Laboratory of Biomedical Magnetic Resonance, ‡Laboratory of Pharmacology and Therapeutics, and §Radiobiology and Radioprotection Unit, Université Catholique de Louvain, Brussels, Belgium

Purpose: To characterize changes in the tumor microenvironment early after irradiation and determine the factors responsible for early reoxygenation.

Methods and Materials: Fibrosarcoma type II (FSaII) and hepatocarcinoma transplantable liver tumor tumor oxygenation were determined using electron paramagnetic resonance oximetry and a fiberoptic device. Perfusion was assessed by laser Doppler, dynamic contrast-enhanced MRI, and dye penetration. Oxygen consumption was determined by electron paramagnetic resonance. The interstitial fluid pressure was evaluated by the wick-in-needle technique.

Results: An increase in oxygen partial pressure was observed 3–4 h after irradiation. This increase resulted from a decrease in global oxygen consumption and an increase in oxygen delivery. The increase in oxygen delivery was due to radiation-induced acute inflammation (that was partially inhibited by the antiinflammatory agent diclofenac) and to a decrease in interstitial fluid pressure. The endothelial nitric oxide synthase pathway, identified as a contributing factor at 24 h after irradiation, did not play a role in the early stage after irradiation. We also observed that splitting a treatment of 18 Gy into two fractions separated by 4 h (time of maximal reoxygenation) had a greater effect on tumor regrowth delay than when applied as a single dose.

Conclusion: Although the cell cycle redistribution effect is important for treatment protocols using multiple daily radiation fractions, the results of this work emphasize that the oxygen effect must be also considered to optimize the treatment strategy.

Tumor oxygenation, Electron paramagnetic resonance, Magnetic resonance imaging, Tumor microenvironment, Radiotherapy.

INTRODUCTION

As an alternative to radiotherapy regimens regarded as "conventional" (fractionated doses of 1.8–2.2 Gy given once daily, 5 d/wk for about 7 weeks), altered fractionation schedules using multiple daily radiation fractions have been proposed as a promising strategy to treat rapidly proliferating tumors (1). These protocols include hyperfractionation and accelerated fractionation. Generally, a therapeutic gain for these regimens is expected for the patient as long as acute reactions remain tolerable and later effects are unchanged. The aim of accelerated fractionation is to minimize the potential for tumor growth or regeneration during therapy (2). Moreover, the therapeutic gain could exploit the sensitization due to the cell cycle redistribution (1–4).

The dynamic changes in the tumor microenvironment have been largely ignored as factors that may contribute to greater radiosensitivity of tumors in the protocols that use multiple daily fractions. This is very different from the classic "reoxygenation effect" described for conventional radiotherapy regimens. A large amount of evidence has shown that the reoxygenation of tumors occurs 24–72 h after irradiation (5–15). It has been shown that

Reprint requests to: Bernard Gallez, Ph.D., CMFA/REMA, Avenue Mounier 73.40, Brussels B-1200 Belgium. Tel: (+32) 2-764-2792; Fax: (+32) 2-764-2790; E-mail: Gallez@cmfa.ucl.ac.be

Supported by Grants from the Belgian National Fund for Scientific Research (FNRS), Fonds Joseph Maisin, and "Actions de Recherches Concertées-Communauté Française de Belgique-ARC 04/09-317;" R. A. and J. D. W. are FNRS-Televie Fellows; P. S., C. B., and B. J. are Research Fellows of the FNRS; O. F. is a Research Associate of the FNRS.

Acknowledgments—The authors thank Guerbet Laboratories (Roissy, France) for providing P792.

Received Aug 12, 2004, and in revised form Jan 19, 2005. Accepted for publication Feb 21, 2005.

this late reoxygenation contributes significantly to the efficacy of a second irradiation (12, 15). The molecular basis of reoxygenation at 24 h was recently investigated. It turns out to be mediated by nitric oxide, following changes in expression and activity of endothelial nitric oxide synthase (eNOS) and caveolin, with a consequent increase in blood flow and oxygen delivery (15).

In contrast to the "late" reoxygenation effect, which occurs 1 or 2 days after irradiation, little is known about the changes in the microenvironment at early stages just after irradiation. In pioneering studies, Kallman (16) and Dorie (17) suggested that the phenomenon of reoxygenation could be caused by the reacquisition of radiosensitivity by those cells that are able to survive irradiation because they were hypoxic at exposure. They described a rather rapid phenomenon in several tumor lines. The indirect evidence of reoxygenation was based on the determination of the hypoxic fraction using dose-survival curves of suspended cells taken from irradiated tumors. They found that the hypoxic fraction had already declined 1 h after a single radiation fraction of 10 Gy (16, 17). Later, the development of oximetry technologies allowed direct *in vivo* measurements of oxygen partial pressure (pO_2). Using ^{19}F-nuclear magnetic resonance relaxometry, pO_2 measurements suggested a reoxygenation at 1, 4, and 10 h after irradiation of 20 Gy (18). To our knowledge, the only study that has measured pO_2 early after irradiation using a clinically relevant dose (2 Gy) was by Weissfloch *et al.* (19) with the Eppendorf system. They showed an increase in tumor oxygenation 2 h after irradiation and a decrease at 24 h after irradiation (19). To our knowledge, no study has described a continuous measurement of tumor oxygenation to determine the time sequence and extent of reoxygenation in tumors early after irradiation.

We hypothesized that early tumor reoxygenation, in addition to the cell cycle redistribution effect, might significantly contribute to the radiosensitivity of tumor cells in radiotherapy protocols that use multiple daily fractions. Therefore, we determined the time sequence of reoxygenation in two experimental tumor models. These measurements were performed using recently developed oximetry technologies: electron paramagnetic resonance (EPR) oximetry and the OxyLite system (Oxford Optronix, Oxford, UK). Both methods allow continuous measurements of pO_2 from the same site in tumors for long periods (20–26). EPR oximetry was previously used to monitor the changes in pO_2 late after irradiation (8, 9, 11, 12, 15), but never at the early stages after irradiation. We observed that oxygenation was dramatically increased early after a 2-Gy fraction, with a maximal pO_2 reached about 4 h after irradiation. At maximal reoxygenation, we characterized the changes in the tumor microenvironment to determine the factors responsible for this early reoxygenation.

METHODS AND MATERIALS

Animal tumor models

Two different syngeneic tumor models were implanted in the gastrocnemius muscle in the rear leg of male mice (20–25 g, B&K, Hull, UK): the transplantable liver tumor TLT in MRI mice and the FSaII tumor in C3H mice. All treatments were applied when the tumors reached 8.0 ± 0.5 mm. All experiments were conducted according to national animal care regulations.

Treatments

The animals were anesthetized by inhalation of isoflurane mixed with 21% oxygen in a continuous flow (1.5 L/h), delivered by a nose cone. Initiation of anesthesia was performed using 3% isoflurane. The isoflurane was then stabilized at 1.2% during a minimum of 15 min before any measurement. The temperature of the animals was kept constant using an infrared light or a homeothermic blanket control unit. When the NOS inhibitor L-ω-nitro-L-arginine methyl ester (L-NAME, Sigma, Steinheim, Germany) was used, it was administered in the drinking water (500 mg/L of water) the day before irradiation until the end of the measurements (27). When the nonsteroidal antiinflammatory drug diclofenac was used, it was injected intraperitoneally into the mice 30 min before irradiation (Voltaren, diluted in saline water to a final concentration of 5 mg/mL, 0.5 mg/mice) (28).

Oxygen measurements

Local tumor oxygenation measurements were done using two independent techniques: EPR oximetry and the OxyLite fiberoptic probe system.

EPR oximetry. Electron paramagnetic resonance oximetry (using charcoal as the oxygen sensitive probe) was used to evaluate tumor oxygenation changes using a previously described protocol (29, 30). EPR spectra were recorded using an EPR spectrometer (Magnettech, Berlin, Germany) with a low-frequency microwave bridge operating at 1.2 GHz and an extended loop resonator. Mice were injected 2 days before EPR analysis in the center of the tumor using the suspension of charcoal (100 mg/mL, 50 μL injected, particle size <25 μm). The EPR study was begun when the tumor reached 8.0 ± 0.5 mm in diameter. These localized EPR measurements record the average pO_2 in a volume of about 10 mm^3 (30).

OxyLite technique. We used the OxyLite system for continuously monitoring tumor oxygenation and temperature at the same location (31). These fiberoptic microprobes combine an oxygen sensor and a thermocouple. The measurement is based on the fluorescence quenching of a ruthenium crystal modulated by the local pO_2. The tip of the probe was inserted into the tumor. Data were collected continuously before, during, and for 6 h after irradiation. OxyLite pO_2 measurements are single point measurements, and the volume sampled is confined to the sensor tip (230 μm in diameter). Braun *et al.* (32) estimated that the probe would measure an average pO_2 in a area of about 40,000 μm^2.

Perfusion measurements

Tumor perfusion was assessed by three complementary techniques: laser Doppler imaging, patent blue staining, and dynamic contrast-enhanced (DCE)-MRI.

Laser Doppler imaging. Superficial tumor perfusion was determined using a laser Doppler imager (Moor Instruments) (15). The skin was depilated the day before the experiment. The mice were placed on a heating pad (37°C). The laser Doppler source was

mounted on a movable rack exactly 20 cm above the mouse limbs. Using these settings, light penetrates the skin and tumor to a maximal depth of 2 mm. In the presence of moving red blood cells in nutritional capillaries, arterioles, and venules, a fraction of the light is Doppler shifted, detected, and converted into a computerized, color-coded image. The mean tumor blood flow was determined from a color pixel histogram using image analysis software (Laser Doppler Perfusion Measure, version 3.0.8, Moor Instruments). For each mouse, perfusion fluxes recorded in the gastrocnemius muscle of the other leg were used as the control.

Patent blue staining. Patent blue (Sigma-Aldrich, Bornem, Belgium) distribution in tumors was used as a rough marker of perfusion and permeability (33). We injected 200 μL of patent blue stain (1.25%) diluted in physiologic saline solution into the tail vein of the mice. After 1 min, the time that corresponded to uniform distribution of the dye throughout the body, the mice were killed, and the tumor was carefully excised and cut into two halves. Each of these two tumor cross-sections was photographed with a digital camera. To compare the stained and nonstained areas, in-house software based on the interactive data language (IDL) (Research Systems, Boulder, CO) was developed. For each tumor cross-section, a region of interest (stained area) was defined and the percentage of stained area of the whole cross-section calculated. The mean percentage of staining was then calculated and used as an indicator of tumor perfusion.

Dynamic contrast-enhanced MRI. Using DCE-MRI, it is possible to provide parametric maps that reflect the plasma volume fraction, permeability, and rate of efflux, as described previously (34). To generate these parametric maps, MRI was performed with a 4.7-T (200 MHz, ^{1}H), 40-cm inner diameter, bore system (Bruker Biospec, Ettlingen, Germany). T_2-weighted anatomic images were acquired using a fast spin echo sequence (TR 4 s, TE 50.5 ms). A single, 1.6-mm-thick slice passing through the tumor center was localized. A birdcage radiofrequency coil with an inner diameter of 70 mm was used for radiofrequency transmission and reception. For the DCE-MRI study, two axial (transverse) slices were selected: one was centered on the kidneys and one was positioned on the tumor. T_1-weighted gradient-recalled echo images were obtained with the following parameters: TR 40 ms, TE 4.9 ms, 1.6-mm slice thickness, flip angle 90°, matrix 64 × 64, field of view 6 cm, 25-kHz receiver bandwidth, resulting in an acquisition time of 2.56 s/scan. The contrast agent was a rapid-clearance blood pool agent, P792 (Vistarem, Laboratoire Guerbet, Aulnay sous Bois, France). P792 (molecular weight 6.47 kD) is a monogadolinium macrocyclic compound based on a gadolinium tetraazacyclododecanetetraacetic acid structure substituted by hydrophilic (dextran) arms. Its R_1 relaxivity in 37°C human serum albumin (HSA), 4% at 4.7 T is 9.0 $mM^{-1}s^{-1}$ (data communicated by Guerbet). P792 was injected at dose of 0.042 mmol gadolinium/kg as recommended by the manufacturer and published studies (35). The DCE study was performed using the following protocol. After 12 baseline images had been acquired, P792 was administered intravenously within 2 s (50 μL/40 g mouse), and the enhancement kinetics were continuously monitored for 8 min (200 total scans). This allowed sampling of the signal intensity curve often enough to track the fast rise in tissue enhancement for viable tumor after bolus arrival. Immediately afterward, a slower DCE data set was acquired to monitor the washout of the contrast agent. For this second set, 60 scans were acquired at a temporal resolution of 60 s (1 h total).

Kinetic analysis

Dynamic contrast enhanced-MRI raw data were zero filled and two-dimensional Fourier transformed, resulting in an in-plane resolution of 128 × 128. An operator-defined region of interest encompassing the tumor was analyzed on a voxel-by-voxel basis to obtain the parametric maps. Voxels showing either no signal enhancement or a linear increase of signal intensity (SI) were excluded from the analysis. This was achieved by identifying voxels with statistically significant variations in T_1-weighted signal intensity using power spectrum analysis. Using cluster analysis, voxels for which typical signal enhancement curves were observed were then selected for pharmacokinetic analysis (36).

The contrast agent concentration as a function of time after P792 injection [C(t)] was estimated by comparing the tumor signal intensity as a function of time [S(t)], with the signal intensity in a reference tissue (muscle) with known T_1 (37). Assuming that the signal intensity changes linearly as a function of contrast media concentration (T_1-weighted sequence, short TE, TR << T1), then

$$C(t) = \frac{1}{R_1 T_{1(muscle)}} \frac{S(t) - S(0)}{S_{muscle}(0)} \quad (1)$$

where R1 is the longitudinal relaxivity of the contrast agent (assumed to be equal to that in HSA 4%) and the T_1 of muscle is assumed to be 900 ms. The tracer concentration changes were fitted to a two-compartment pharmacokinetics model (37, 38). In this model, the contribution of the tracer in the blood plasma to the total tissue concentration is included (negligible in blood–brain barrier lesions but often significant in tumors) and different permeability constants for flux into and out of the extravascular extracellular space are allowed. The model assumes that the tracer is well mixed throughout the compartments (tumor regions with high interstitial fluid pressure might not meet this condition) and that a fast exchange of all mobile ^{1}H occurs within the tissue. The model also assumes that the increase in T_1 relaxation rate is proportional to the concentration of the tracer.

The following equation describes the tissue concentration as a function of time:

$$C(t > t0) = K_{in}^{Trans} A0 \cdot \frac{\exp^{\frac{K_{out}^{Trans}}{v_e} t} - \exp^{-kt1}}{k1 - \frac{K_{out}^{Trans}}{v_e}} + v_p \cdot A0 \cdot \exp^{-kt1} \quad (2)$$

where K^{Trans}_{in} is the influx volume transfer constant (into extravascular extracellular space from plasma), K^{Trans}_{out} is the efflux volume transfer constant (from extravascular extracellular space back to plasma), v_e is the volume of extravascular extracellular space per unit volume of tissue, and v_p is the blood plasma volume per unit volume of tissue. K^{Trans}_{out} and v_e cannot be estimated separately, thus only k_{ep}, the ratio K^{Trans}_{out}/v_e, is calculated. k_{ep} is the fractional rate of efflux from the interstitial space back to the blood. The constants used in the fitting are the maximal concentration of P792 in the plasma (A0), the blood decay rate (k1), and the time to the maximal tracer plasma concentration t_0. It is assumed that the rapid enhancement phase (from t = 0 to t0) is primarily due to intravascular contrast media during the first pass of the contrast media bolus, and the slower phase is due to leakage into the extracellular space. A universal t0 time value was estimated for each mouse from the kidney data. Additionally, the

decay rate of the contrast agent in the bloodstream was estimated from the enhancement kinetics in one or two selected renal cortex voxels showing early and large [P792] signal enhancement, presumably reflecting pronounced arterial perfusion. A monoexponential function was fit to the [P792] kidney. Fitting was performed using a Levenberg-Marquardt nonlinear least-squares procedure. Parametric images for K^{Trans}_{in}, v_p, and k_{ep} were computed, with only the statistically significant parameter estimates displayed.

Interstitial fluid pressure measurements

The interstitial fluid pressure (IFP) was measured using a "wick-in-needle" apparatus (39, 40). An 18-gauge needle with a 1-mm side hole located at about 5 mm from the needle tip was connected to the Stryker pressure monitor system (Stryker, 295-1 Pressure; Stryker Corporation, Kalamazoo, MI), specially designed for measuring tissue fluid pressures. The entire system was filled with saline water. The calibration of the pressure was checked before each experiment. A zero reference was obtained by placing the needle to one side at tumor height and by resetting the system. The needle was inserted approximately into the center of the tumor, then 50 μL of saline was injected to measure IFP.

Tumor regrowth delay assay

The FSaII tumor (8.0 ± 0.5 mm) was locally irradiated with a 250-kV X-ray irradiator (RT 250, Philips Medical System, 1.2 Gy/min). The tumor was centered in a 3-cm-diameter circular irradiation field. After treatment, the tumor diameter was measured daily using a digital caliper until the diameter reached 16 mm, at which time the mice were killed. A linear fit was performed for diameters ranging from 8 to 16 mm, allowing determination of the time to reach a particular size for each mouse.

Oxygen consumption rate evaluation

An EPR method was used that has been previously described (20, 21). In brief, the spectra were recorded on a Bruker EMX EPR spectrometer operating at 9 GHz. The mice were killed and the tumors excised and trypsinized for 30 min, and cell viability was determined with trypan blue exclusion. Cells (2×10^7/mL) were suspended in 10% dextran in complete medium. A neutral nitroxide, ^{15}N 4-oxo-2,2,6,6-tetramethylpiperidine-d_{16}-^{15}N-1-oxyl at 0.2 mM (CDN Isotopes, Pointe-Claire, Quebec, Canada), was added to 100-μL aliquots of tumor cells that were then drawn into glass capillary tubes. The probe (0.2 mM in 20% dextran in complete medium) was calibrated at varying oxygen levels between 100% nitrogen and air so that the line width measurements could be related to oxygen at any value. Nitrogen and air were mixed in an Aaborg gas mixer, and the oxygen content was analyzed using a Servomex oxygen analyzer (OA540; Servomex, Crowborough, East Sussex, UK). The sealed tubes were placed into quartz EPR tubes and the samples maintained at 37°C. Because the resulting line width reports on pO_2, it was possible to calculate the oxygen consumption rates by measuring the pO_2 in the closed tube as a function of time and subsequently computing the slope of the resulting plot.

Experimental design

Oximetry. pO_2 was measured by EPR oximetry 1 h before irradiation (basal value) and at 1, 2, 3, 4, 5, 6, 24, 48, and 72 h after irradiation. The measurements were done in four groups of FSaII tumors: one control group ($n = 10$) and three irradiated groups of 2 Gy ($n = 5$), 9 Gy ($n = 7$), and 25 Gy ($n = 7$). For TLT tumors, one control group ($n = 6$) and the 2-Gy irradiated group ($n = 8$) were used. pO_2 measurements were also done in the gastrocnemius muscle of the C3H mice ($n = 4$) before and after 2-Gy irradiation. Additionally, pO_2 was measured continuously using OxyLite in FSaII tumors from 1 h before to up to 5 h after irradiation at 2 Gy ($n = 4$) and 25 Gy ($n = 6$). In the fractionated protocol, two groups of FSaII mice were used: one control group ($n = 4$) and one group irradiated twice with 2 Gy, the interval between fractions was 4 h ($n = 5$). pO_2 was measured by EPR oximetry 1 h before irradiation and each hour after the first irradiation.

L-NAME treatment. pO_2 was measured by EPR oximetry each hour before and after irradiation in two groups of FSaII ($n = 5$) and TLT ($n = 6$) tumors. All the mice were treated by L-NAME 1 day before irradiation of 2 Gy.

Diclofenac treatment. Electron paramagnetic resonance oximetry was performed in FSaII tumors: one group was irradiated with 2 Gy ($n = 7$) and a second group was pretreated with diclofenac 30 min before 2-Gy irradiation ($n = 8$). pO_2 was measured 1 h before (basal value) and 4 h after irradiation.

Laser Doppler imaging. Perfusion at the surface of the tumor was measured in the FSaII tumors before and 4 h after 2-Gy irradiation ($n = 6$).

Patent blue staining. Two groups of FSaII tumors were used: one control group ($n = 5$) and one group 4 h after 2-Gy irradiation ($n = 6$).

Dynamic contrast-enhanced MRI. Two groups of FSaII tumors were used: one control group ($n = 4$) and one group measured 4 h after 2 Gy irradiation ($n = 4$).

Interstitial fluid pressure. Two groups of FSaII tumors were used: one control group ($n = 5$) and one group 4 h after 2-Gy irradiation ($n = 5$).

Oxygen consumption. These experiments were performed on the FSaII tumors. The consumption rate was determined on the same number of cells (dead and alive) from control tumors ($n = 5$) and irradiated tumors ($n = 4$).

Tumor regrowth delay. Three groups of FSaII tumors were used. The first group ($n = 4$) was irradiated once with a single 18-Gy dose, the second group ($n = 4$) was irradiated twice with two fractions of 9 Gy separated by 4 h, and the third group ($n = 4$) was not irradiated.

RESULTS

Reoxygenation time sequence

The two oximetry techniques used in this study are designed for continuous measurement of local pO_2 without altering the local oxygen concentration (i.e., these are non–oxygen-consuming methods). They allow real-time studies of oxygen fluctuations in tissues. OxyLite probes allow continuous measurement for several hours, and EPR oximetry allows repeated measurements from the same site for days and weeks. In this study, we observed that irradiation of tumors at therapeutically relevant single doses (2 Gy) dramatically modified the tumor oxygenation. Significant changes were observed in the two tumor models compared with the nonirradiated tumors. The increase in pO_2 began early, reaching a plateau after about 3–4 h. These pO_2 values remained elevated for up to 24 h in the FSaII tumor model and even longer in the TLT tumor model (Fig. 1A,B).

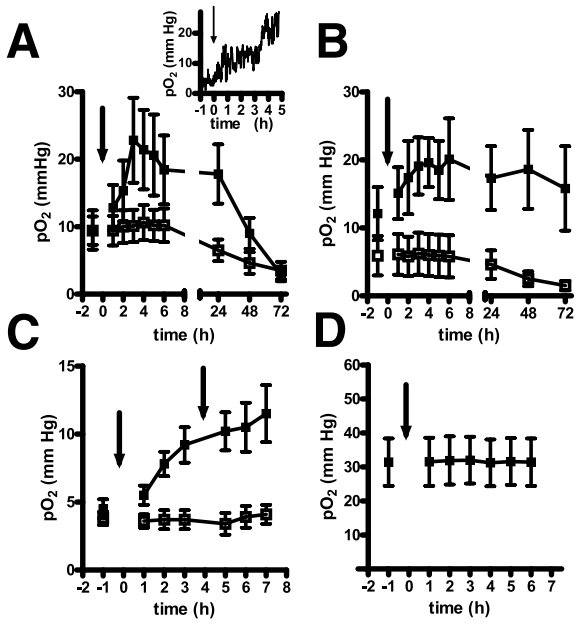

Fig. 1. Effect of irradiation on tumor pO_2. (A) pO_2 measured by electron paramagnetic resonance (EPR) oximetry in two groups of fibrosarcoma type II (FSaII) tumors: control ($n = 10$) and those receiving 2-Gy fraction ($n = 5$). Arrow indicates time of irradiation. (Insert) Typical pO_2 monitoring by OxyLite system in FSaII tumor irradiated with 2 Gy. (B) pO_2 measured by EPR oximetry in two groups of transplantable liver tumor tumors: control ($n = 6$) and those receiving 2-Gy fraction ($n = 8$). (C) pO_2 measured by EPR oximetry in two groups of FSaII tumors: control ($n = 4$) and those irradiated twice with 4-h delay ($n = 5$). Arrow indicates time of irradiation. (D) pO_2 measured by EPR oximetry in gastrocnemius muscle of C3H mice ($n = 4$) before and up to 6 h after 2-Gy fraction.

In the FSaII tumor model, a similar effect was also observed for doses of 9 and 25 Gy (data not shown). For experiments involving two fractions, we observed an increase in pO_2 after the first fraction, and the pO_2 remained elevated after the second fraction (Fig. 1C). Contrary to the effect observed in tumors, irradiation of the gastrocnemius muscle of the mice did not lead to changes in the basal pO_2 (Fig. 1D). Because the maximal tumor pO_2 was attained 4 h after irradiation, we selected this time to characterize other parameters of the tumor microenvironment to identify possible origins for this early reoxygenation.

Effect of irradiation on tumor perfusion

All three techniques used to estimate tumor perfusion indicated that it was increased 4 h after 2 Gy of irradiation. A significant increase of 31.2% ± 6.0% (mean ± standard error, $p < 0.05$, Student's t test) in superficial tumor blood flow was observed using laser Doppler imaging (Fig. 2A). Using patent blue staining, we observed an increase of 111.4% ± 11.0% ($p < 0.05$) of the colored area in the tumor sections 4 h after irradiation (Fig. 2B). Using DCE-MRI, it was possible to create parametric maps that reflected the plasma volume fraction, permeability, and rate of efflux. Typical maps for these parameters are shown in Fig. 3. A significant increase ($p < 0.01$) in the plasma volume fraction (v_p) was observed 4 h after 2 Gy of irradiation compared with the control group. Permeability and the fractional rate of efflux were not significantly changed 4 h after irradiation ($p > 0.05$; Fig. 3).

Effect of irradiation on tumor IFP

Using the wick-in-needle technique, we observed that the IFP was reduced by 25% 4 h after irradiation ($p < 0.001$, Student's t test). The IFP in the tumor center was 19.0 ± 0.4 mm Hg and 14.0 ± 0.7 mm Hg (mean ± standard error) for the control and irradiated group, respectively.

Effect of irradiation on oxygen consumption rate

Global oxygen consumption was significantly reduced after irradiation (Fig 4). The slope for the irradiated group was significantly lower than that for control group ($p < 0.001$, Student's t test) 4 h after 2 Gy of irradiation. This decrease in global consumption was due (at least in part) to an increase in the number of dead cells: 13.8% ± 0.9% for control tumors and 19.9% ± 0.7% for those irradiated with 2 Gy.

Involvement of NOS pathway

It was previously described that the reoxygenation observed 24 h after irradiation was dependent on the relative

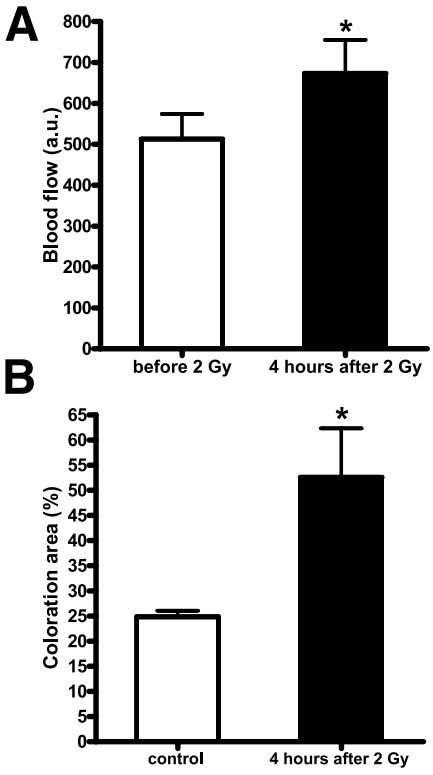

Fig. 2. Effect of irradiation on tumor blood flow 4 h after single dose of 2 Gy. (A) Measured by laser Doppler imaging in fibrosarcoma type II (FSaII) tumors ($n = 6$). Mean ± SEM; bilateral Student's t test; white squares, before 2 Gy; black squares, 4 h after 2 Gy. (B) Coloration area measured by patent blue staining in FSaII tumors. Mean ± SEM; bilateral Student's t test; white squares, control ($n = 5$); black squares, 4 h after 2 Gy ($n = 6$).

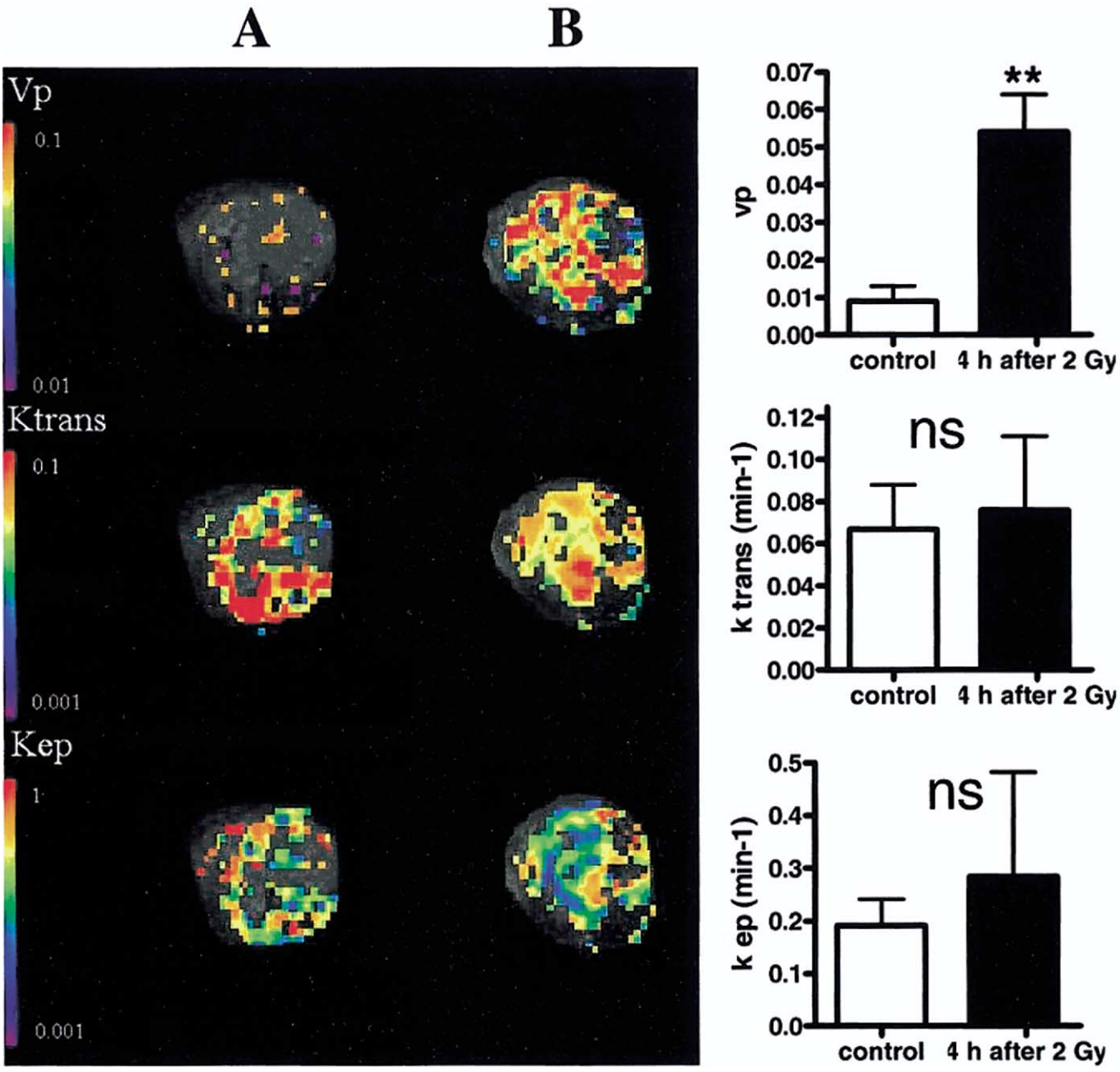

Fig. 3. Effect of irradiation on blood flow and tumor permeability estimated by dynamic contrast enhanced-magnetic resonance imaging (DCE-MRI) on fibrosarcoma type II (FSaII) tumors shown in parametric maps. Typical perfusion (v_p), permeability (K_{trans}), and efflux rate (K_{ep}) maps of (A) control mouse and (B) mouse 4 h after 2-Gy fraction. Also shown are histograms of perfusion, permeability, and efflux rate. Bilateral Student's *t* test. White bars, control ($n = 4$); black bars, 4 h after 2 Gy ($n = 4$).

abundance of eNOS and on a decrease in caveolin, the physiologic inhibitor of NOS (15). To determine whether this pathway was involved in the early reoxygenation we observed, we used pretreatment with a NOS inhibitor (L-NAME), which has been shown to inhibit the increase in tumor pO_2 24 h after irradiation (15). We did not observe any difference in tumor oxygenation between the control group and the group pretreated with L-NAME during the first 6 h after irradiation. Results obtained before and 4 h after 2 Gy of irradiation are shown in Fig. 5. This contrasts with the increase in pO_2 we observed at 24 h in the TLT tumor model that was significantly inhibited by pretreatment with L-NAME (data not shown), as previously observed by Sonveaux *et al.* (15).

Involvement of an inflammation process

We hypothesized that radiation-induced acute inflammation may contribute to the early reoxygenation effect. When treated with diclofenac (a nonsteroidal antiinflammatory drug) 30 min before a 2-Gy fraction, the tumor pO_2 was

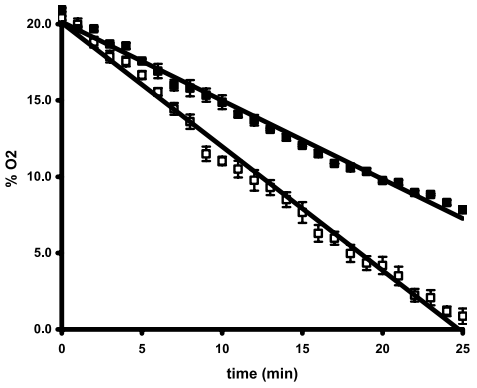

Fig. 4. Effect of irradiation on global oxygen consumption of fibrosarcoma type II (FSaII) tumors. White squares, control (n = 5); black squares, 4 h after 2 Gy (n = 4). Oxygen rate measured as function of time (mean ± SEM). Slope for irradiated group significantly lower than that for control group ($p < 0.001$, Student's t test) 4 h after 2-Gy fraction.

greater than before irradiation, but the pO_2 reached was significantly lower ($p < 0.01$, two-way analysis of variance) than that observed in the untreated group (Fig. 6).

Effect of fractionated doses on tumor regrowth delay

To assess the relevance of early reoxygenation as a factor of radiosensitivity, we compared the regrowth delay of tumors irradiated by one dose of 18 Gy or two doses of 9 Gy separated by a delay of 4 h for maximal reoxygenation. The time for the tumor to reach 12 mm was 3.9 ± 0.2 days for the control group, 7.0 ± 0.2 days for the group that received one fraction, and 8.8 ± 0.5 days for the group that received two fractions. The regrowth delay for the group that received fractionated doses (4.9 ± 0.8 days) was significantly

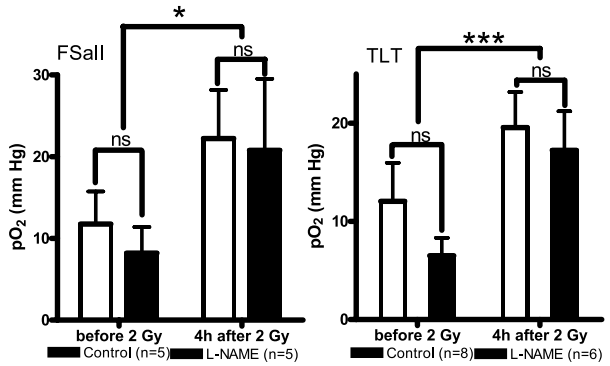

Fig. 5. Effect of L-NAME on pO_2 4 h after tumor irradiation. (left) fibrosarcoma type II (FSaII) model and (right) transplantable liver tumor (TLT) model. Irradiation caused significant increase in tumor pO_2 in both groups (FSaII, $p < 0.05$; TLT, $p < 0.001$, two-way repeated measures analysis of variance). When L-NAME was combined with irradiation, increase in tumor pO_2 was not significantly lower than for control group ($p > 0.05$, two-way repeated measures analysis of variance). Basal tumor pO_2 was same in both groups ($p > 0.05$, two-way repeated measures analysis of variance). pO_2 measured by EPR oximetry (mean ± SEM).

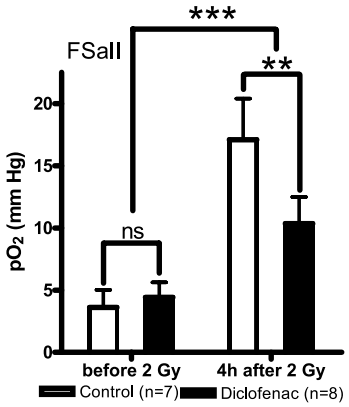

Fig. 6. Effect of diclofenac on the pO_2 4 h after tumor irradiation. Irradiation caused significant increase in tumor pO_2 in both groups ($p < 0.001$, two-way repeated measures analysis of variance). However, when diclofenac was combined with irradiation (diclofenac-treated, black bars, n = 8), tumor pO_2 increase was significantly lower than for control group (white bars, n = 7; $p < 0.01$, two-way repeated measures analysis of variance). Basal tumor pO_2 same in both groups ($p > 0.05$, two-way repeated measures analysis of variance). Data shown as mean ± SEM.

greater ($p < 0.05$) than that for the group that received one fraction (3.1 ± 0.4 days).

DISCUSSION

Revisiting "reoxygenation effect" and factors responsible for it

The hypothesis of reoxygenation of tumors after irradiation was proposed more than three decades ago (40). After irradiation, which is expected to eliminate preferentially the well-oxygenated cells, it was assumed that continuous movement of previously anoxic cells into the category of well-oxygenated cells should occur (41). This hypothesis was supported by measurements of hypoxic fraction via the paired survival curve technique (16, 17, 41). Later, after the development of convenient oximetry technologies, the evidence for this reoxygenation was confirmed. However, most studies focused on relatively long delays (24–48 h after irradiation). Moreover, data showing evidence of earlier reoxygenation were generally only obtained for one time point and high irradiation doses (18, 42, 43). For the first time, we report the timing sequence of reoxygenation by continuous measurement of pO_2 in two tumor models after irradiation using a clinically relevant dose (2 Gy). We observed a rapid phenomenon that occurred in the first 3–4 h after irradiation, with the pO_2 remaining elevated for at least 24 h. The reoxygenation effect was maintained after a second irradiation dose given 4 h after the first fraction. Having identified the sequence of reoxygenation, we then used multiple modalities to characterize the possible mechanisms responsible for this effect. Tumor reoxygenation may result from an increase in oxygen delivery and/or a decrease in oxygen consumption by the tumor cells (42). Our data confirmed that both of these mechanisms play a role in reoxygenation in the tumor models studied. Moreover, having identified

the determining factors for each of these mechanisms, it is possible to discuss the possible relevance for human tumors.

Improved blood flow is responsible for early tumor reoxygenation. All methods used to assess tumor perfusion consistently showed an increase at 4 h after irradiation. These results are consistent with those of other studies showing an increase in tumor perfusion at 24 and 48 h after irradiation (11, 15, 44). This increase in tumor perfusion parallels a decrease in IFP that was measured at the same time using the wick-in-needle technique. A decrease in IFP after greater doses of irradiation (10 Gy) was described by Znati *et al.* (10). That group suggested that a decrease in venous vascular resistance could result from a reduction in the compression of venous vessels by cancer cells. In our previous study on the mechanisms responsible for the increase in tumor perfusion 24 h after irradiation, Sonveaux *et al.* (15) demonstrated that the improvement in tumor circulation was nitric oxide mediated with changes in expression of eNOS and caveolin, with a consequent increase in blood flow and oxygen delivery. However, this mechanism is apparently not involved in the early stage of reoxygenation, because it was not abolished by the administration of L-NAME. The time necessary to observe a change in the expression of eNOS and caveolin (15) is consistent with these observations. It is likely that the NO pathway relays the initial reoxygenation and is responsible for a prolonged effect. Nevertheless, the decrease in IFP is not the sole factor responsible for the improved tumor blood flow. We showed that an inflammation process also participated in the reoxygenation. An inflammatory process is known to occur rapidly after irradiation (45, 46), thereby causing an increase in blood flow by vasorelaxation. Using diclofenac as an antiinflammatory agent, we observed a significant decrease in the level of tumor oxygenation 4 h after irradiation. However, the reoxygenation effect was only partially abolished, indicating that other factors are responsible for this increase in tumor oxygenation. We also found a significant decrease in the global oxygen consumption rate. The cell loss observed after irradiation was significant at 4 h after irradiation and was partly responsible for this effect. A reduced oxygen metabolism by the surviving cells (actually fixing trypan blue) may also be involved in this decrease in oxygen consumption. Thus, we can now propose a likely scenario for the early reoxygenation effect of tumors on the basis of the factors identified in the present study (Fig. 7).

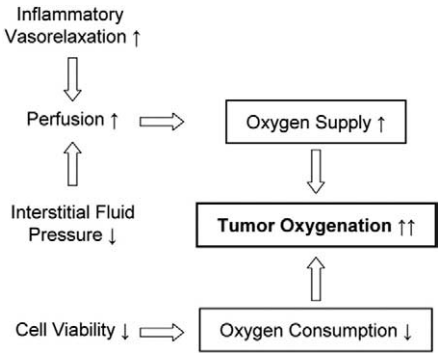

Fig. 7. Factors contributing to early reoxygenation effect. Increase in tumor oxygenation due to decrease in oxygen consumption and increase in oxygen supply. Decrease in oxygen consumption partly attributed to reduction in net number of tumors cells. Increase in oxygen delivery attributed to decrease in interstitial fluid pressure and radiation-induced acute inflammation. Endothelial nitrous oxide synthase pathway, identified as contributing factor at 24 h after irradiation, did not play significant role in early stage after irradiation.

Consequences of reoxygenation and relevance for other tumor types

Oxygen is the most potent chemical modifier of radiosensitivity, and many therapeutic interventions, such as breathing oxygen-enriched gas, using vasoactive agents (30), or using inhibitors of tumor oxygen consumption (22, 47), are under investigation. Although the reoxygenation effect has been presented in most textbooks as a key factor for the enhancement of radiosensitivity in conventional fractionated regimens, this factor has generally been neglected in protocols that use several fractions daily. The most cited factor for a gain in treatment efficacy is the redistribution of the cell cycle. We have demonstrated that the oxygen effect is likely to be another major contributing factor in the therapeutic efficacy of accelerated radiotherapy. We observed an increased efficacy of fractionation in two doses separated by 4 h, the time of maximal reoxygenation in this tumor model. The dose used for that experiment (18 Gy) was within the range of doses (2–25 Gy) for which we observed a similar reoxygenation effect. What is the relevance of our findings for other experimental tumors and human tumors? The initial increase in pO_2 observed after irradiation was similar in both tumor types that we studied. The duration of the effect was at least 24 h in one model and 72 h in the other. We observed a similar time to reach the maximal pO_2 in both tumor models. This was likely a coincidence, because others found different kinetics for the reoxygenation using greater radiation doses (6, 9). We identified several key factors responsible for the reoxygenation effect. The same factors should also affect the timing of reoxygenation. Oxygen consumption was involved in tumor reoxygenation. Tumor cell loss was at least partly responsible for this effect. Even if it is expected that the effect on tumor growth is mainly linked to clonogenic death, it should be noted that the cell loss was already significant 4 h after irradiation in this rapidly proliferating tumor. The kinetics of the effect should be dependent on the proliferation rate of the tumor. This is relevant for all experimental tumors and human tumors. For the latter, it is likely that the reoxygenation effect due to tumor cell loss will be delayed, except for tumors characterized by very high proliferation rates. We also observed that acute inflammation significantly contributed to the tumor reoxygenation effect. This component of the reoxygenation effect should be present in all tumor types. Overall, oxygenation in individual tumors after irradiation will evolve depending on the contribution of each factor. This emphasizes the importance of monitoring of the tumor microenvironment to guide the fractionation schedule. With the considerable improvements and availability of techniques that are able to monitor the tumor microenvironment noninvasively, it is likely that guidance for individual treatments will be clinically applicable in the near future.

Finally, it should be noted that the timing between fractions in patients is also dictated by the need to avoid late side effects (e.g., using intervals of 6 h between fractions). Our study revealed that the tumor reoxygenation effect remained persistent for a long period. This confers a long time window during which the tumor is more radiosensitive than before irradiation.

CONCLUSION

Using oximetry technologies that allow continuous measurement of tumor oxygenation, we identified the sequence of reoxygenation after a 2-Gy fraction in two tumor models. The increase in pO_2 begins as early as 3–4 h after irradiation. The increase in tumor oxygenation is due to a decrease in oxygen consumption and an increase in oxygen supply. The increase in oxygen delivery is due to a decrease in IFP and to radiation-induced acute inflammation. The eNOS pathway, which had been identified as a contributing factor at 24 h after irradiation, does not play a role in the early stage after irradiation. Although the cell cycle redistribution effect is important for treatment protocols using multiple daily fractions, the results of this work emphasize that the oxygen effect must be also considered to optimize the treatment strategy.

REFERENCES

1. Ang KK, Thames HD, Peters LJ. Altered fractionation schedules. In: Perez CA, Brady LW, editors. Principles and practice of radiation oncology. 3rd ed. Philadelphia: Lippincott-Raven; 1997. p. 119–142.
2. Withers HR, McBride WH. Biologic basis of radiation therapy. In: Perez CA, Brady LW, eds. Principles and practice of radiation oncology. 3rd ed. Philadelphia: Lippincott-Raven; 1997. p. 79–118.
3. Pawlik TM, Keyomarsi K. Role of cell cycle in mediating sensitivity to radiotherapy. *Int J Radiat Oncol Biol Phys* 2004;59:928–942.
4. Geldof AA, Plaizier MA, Duivenvoorden I, *et al.* Cell cycle perturbations and radiosensitization effects in human prostate cancer line. *J Cancer Res Clin Oncol* 2003;129:175–182.
5. Vaupel P, Frinak S, O'Hara M. Direct measurement of reoxygenation in malignant mammary tumors after a single large dose of irradiation. *Adv Exp Med Biol* 1984;180:773–782.
6. Kallman RF, Dorie MJ. Tumor oxygenation and reoxygenation during radiation therapy: Their importance in predicting tumor response. *Int J Radiat Oncol Biol Phys* 1986;12:681–685.
7. Koutcher JA, Alfieri AA, Devitt ML, *et al.* Quantitative changes in tumor metabolism, partial pressure of oxygen, and radiobiological oxygenation status postradiation. *Cancer Res* 1992;52:4620–4627.
8. O'Hara JA, Goda F, Liu KJ, *et al.* The pO_2 in a murine tumor after irradiation: An in vivo electron paramagnetic resonance oximetry study. *Radiat Res* 1995;144:222–229.
9. Goda F, O'Hara JA, Rhodes ES, *et al.* Changes of oxygen tension in experimental tumors after a single dose of X-ray irradiation. *Cancer Res* 1995;55:2249–2252.
10. Znati CA, Rosenstein M, Boucher Y, *et al.* Effect of radiation on interstitial fluid pressure and oxygenation in a human tumor xenograft. *Cancer Res* 1996;56:964–968.
11. Goda F, Bacic G, O'Hara JA, *et al.* The relationship between pO_2 and perfusion in two murine tumors after X-ray irradiation: A combined Gd-DTPA dynamic MRI and EPR oximetry study. *Cancer Res* 1996;56:3344–3349.
12. O'Hara J, Goda F, Demindenko E, *et al.* Effect on regrowth delay in a murine tumor scheduling split dose irradiation based on direct pO_2 measurements by electron paramagnetic resonance oximetry. *Radiat Res* 1998;150:549–556.
13. Bussink J, Kaanders JH, Rijken PF, *et al.* Changes in blood perfusion and hypoxia after irradiation of a human squamous cell carcinoma xenograft tumor line. *Radiat Res* 2000;153:398–404.
14. Fenton B, Lord E, Paoni S. Effect of radiation on tumor intravascular oxygenation, vascular configuration, development of hypoxia, and clonogenic survival. *Radiat Res* 2001;155:360–368.
15. Sonveaux P, Dessy C, Brouet A, *et al.* Modulation of the tumor vasculature functionality by ionizing radiation accounts for tumor radiosensitization and promotes gene delivery. *FASEB J* 2002;16:1979–1981.
16. Kallman RF. The phenomenon of reoxygenation and its implications for fractionated radiotherapy. *Radiology* 1972;105:135–142.
17. Dorie MJ, Kallman RF. Reoxygenation in the RIF-1 tumor. *Int J Radiat Oncol Biol Phys* 1984;10:687–693.
18. Mason RP, Hunjan S, Le D, *et al.* Regional tumor oxygen tension: Fluorine echo planar imaging of hexafluorobenzene reveals heterogeneity of dynamics. *Int J Radiat Oncol Biol Phys* 1998;42:747–750.
19. Weissfloch L, Auberger T, Feldmann HJ, *et al.* Oxygen tension in isotransplanted mammary carcinomas and osteosarcomas before and after irradiation. *Adv Exp Med Biol* 1996;388:495–504.
20. Jordan BF, Misson PD, Demeure R, *et al.* Changes in tumor oxygenation/perfusion induced by the NO donor, isosorbide dinitrate, in comparison with carbogen: Monitoring by EPR and MRI. *Int J Radiat Oncol Biol Phys* 2000;48:565–570.
21. Jordan BF, Beghein N, Aubry M, *et al.* Potentiation of radiation-induced regrowth delay by isosorbide dinitrate in FSaII murine tumors. *Int J Cancer* 2003;103:138–141.
22. Jordan BF, Gregoire V, Demeure RJ, *et al.* Insulin increases the sensitivity of tumors to irradiation: Involvement of an increase in tumor oxygenation mediated by a nitric-oxide dependent decrease of tumor cells oxygen consumption. *Cancer Res* 2002;62:3555–3561.
23. Jordan BF, Sonveaux P, Feron O, *et al.* Nitric oxide-mediated increase in tumor blood flow and oxygenation of tumors implanted in muscles stimulated by electric pulses. *Int J Radiat Oncol Biol Phys* 2003;55:1066–1073.
24. Jordan BF, Sonveaux P, Feron O, *et al.* Nitric oxide as radiosensitizer: Evidence for an intrinsic role additive to its effect on oxygen delivery and consumption. *Int J Cancer* 2004;109:768–773.
25. Gallez B, Baudelet C, Jordan BF. Assessment of tumor oxygenation by electron paramagnetic resonance: Principles and applications. *NMR Biomed* 2004;17:240–262.
26. Swartz HM, Khan N, Buckey J, *et al.* Clinical applications of EPR: Overview and perspectives. *NMR Biomed* 2004;17:335–351.
27. Sonveaux P, Brouet A, Havaux X, *et al.* Irradiation-induced angiogenesis through the up-regulation of the nitric oxide pathway: Implications for tumor radiotherapy. *Cancer Res* 2003;63:1012–1019.
28. Hoferova Z, Fedorocko P, Hofmanova J, *et al.* The effect of nonsteroidal antiinflammatory drugs ibuprofen, flurbiprofen,

and diclofenac on *in vitro* and *in vivo* growth of mouse fibrosarcoma. *Cancer Invest* 2002;20:490–498.
29. Jordan BF, Baudelet C, Gallez B. Carbon-centered radicals as oxygen sensors for *in vivo* electron paramagnetic resonance: Screening for an optimal probe among commercially available charcoals. *MAGMA* 1998;7:121–129.
30. Gallez B, Jordan BF, Baudelet C, *et al.* Pharmacological modifications of the partial pressure of oxygen in murine tumors: Evaluation using *in vivo* EPR oximetry. *Magn Reson Med* 1999;42:627–630.
31. Baudelet C, Gallez B. How does blood oxygen level-dependent (BOLD) contrast correlate with oxygen partial pressure (pO_2) inside tumors? *Magn Reson Med* 2002;48:980–986.
32. Braun RD, Lanzen JL, Snyder SA, *et al.* Comparison of tumor and normal tissue oxygen tension measurements using OxyLite or microelectrodes in rodents. *Am J Physiol* 2001;280: H2533–H2544.
33. Sersa G, Cemazar M, Miklavcic D, *et al.* Tumor blood flow modifying effect of electrochemotherapy with bleomycin. *Anticancer Res* 1999;19:4017–4022.
34. Baudelet C, Ansiaux R, Jordan BF, *et al.* Physiological noise in murine solid tumor using T_2-weighted gradient-echo imaging: A marker of tumour acute hypoxia? *Phys Med Biol* 2004;49:3389–3411.
35. Fan X, Medved M, River JN, *et al.* New model for analysis of dynamic contrast enhanced MRI data distinguishes metastatic from nonmetastatic transplanted rodent prostate tumors. *Magn Reson Med* 2004;51:487–494.
36. Baudelet C, Gallez B. Cluster analysis of BOLD fMRI time series in tumors to study the heterogeneity of hemodynamic response to treatment. *Magn Reson Med* 2003;49:985–990.
37. Tofts PS. Modeling tracer kinetics in dynamic Gd-DTPA MR imaging. *J Magn Reson Imaging* 1997;7:91–101.
38. Tofts PS, Brix G, Buckley DL, *et al.* Estimating kinetic parameters from dynamic contrast-enhanced T(1)-weighted MRI of a diffusable tracer: Standardized quantities and symbols. *J Magn Reson Imaging* 1999;10:223–232.
39. Fadnes HO, Reed RK, Aukland K. Interstitial fluid pressure in rats measured with a modified wick technique. *Microvasc Res* 1977;14:27–36.
40. Boucher Y, Kirkwood JM, Opacic D, *et al.* Interstitial hypertension in superficial metastatic melanomas in humans. *Cancer Res* 1991;51:6691–6649.
41. Van Putten LM, Kallman RF. Oxygenation status of a transplantable tumor during fractionated radiation therapy. *J Natl Cancer Inst* 1968;40:441–451.
42. Olive PL. Radiation-induced reoxygenation in the SCCVII murine tumour: Evidence for a decrease in oxygen consumption and an increase in tumour perfusion. *Radiother Oncol* 1994;32:37–46.
43. Grau C, Overgaard J. The influence of radiation dose on the magnitude and kinetics of reoxygenation in a C3H mammary carcinoma. *Radiat Res* 1990;122:309–315.
44. Dewhirst MW, Olivier R, Tso CY, *et al.* Heterogeneity in tumor microvascular response to radiation. *Int J Radiat Oncol Biol Phys* 1990;18:559–568.
45. Moore AH, Olschowka JA, Williams JP, *et al.* Radiation-induced edema is dependent on cyclooxygenase 2 activity in mouse brain. *Radiat Res* 2004;161:153–160.
46. el-Ghazaly M, Kenawy S, Khayyal MT, *et al.* Effect of exposure to radiation on the inflammatory process and its influence by diclofenac. *Br J Pharmacol* 1985;85:45–50.
47. Snyder SA, Lanzen JL, Braun RD, *et al.* Simultaneous administration of glucose and hyperoxic gas achieves greater improvement in tumor oxygenation than hyperoxic gas alone. *Int J Radiat Oncol Biol Phys* 2001;51:494–506.